Supporting Information for:

Hotspots in an obligate homodimeric cancer target. Structural and functional effects of interfacial mutations in human thymidylate synthase

Outi M. H. Salo-Ahen[a†], Anna Tochowicz[b†], Cecilia Pozzi[c], Daniela Cardinale[d], Stefania Ferrari[d], Yap Boum[e], Stefano Mangani[c], Robert M. Stroud[b], Hannu Myllykallio[e], Maria Paola Costi[d,*], Glauco Ponterini[d,*], Rebecca C. Wade[a,f,*]

[a]Molecular and Cellular Modeling Group, Heidelberg Institute for Theoretical Studies, 69118 Heidelberg, Germany

[b]Biochemistry and Biophysics Department, University of California San Francisco, San Francisco, CA, USA

[c]Department of Biotechnology, Chemistry and Pharmacy, University of Siena, 53100 Siena, Italy

[d]Department of Life Sciences, University of Modena and Reggio Emilia, 41125 Modena, Italy

[e]Ecole Polytechnique, CNRS UMR7645 - INSERM U696, Palaiseau, France

[f]Center for Molecular Biology, DKFZ-ZMBH Alliance and Interdisciplinary Center for Scientific Computing (IWR), Heidelberg University, 69120 Heidelberg, Germany

Content

Supplemental Figures and Legends

Supporting Tables

Supplemental Figures and Legends

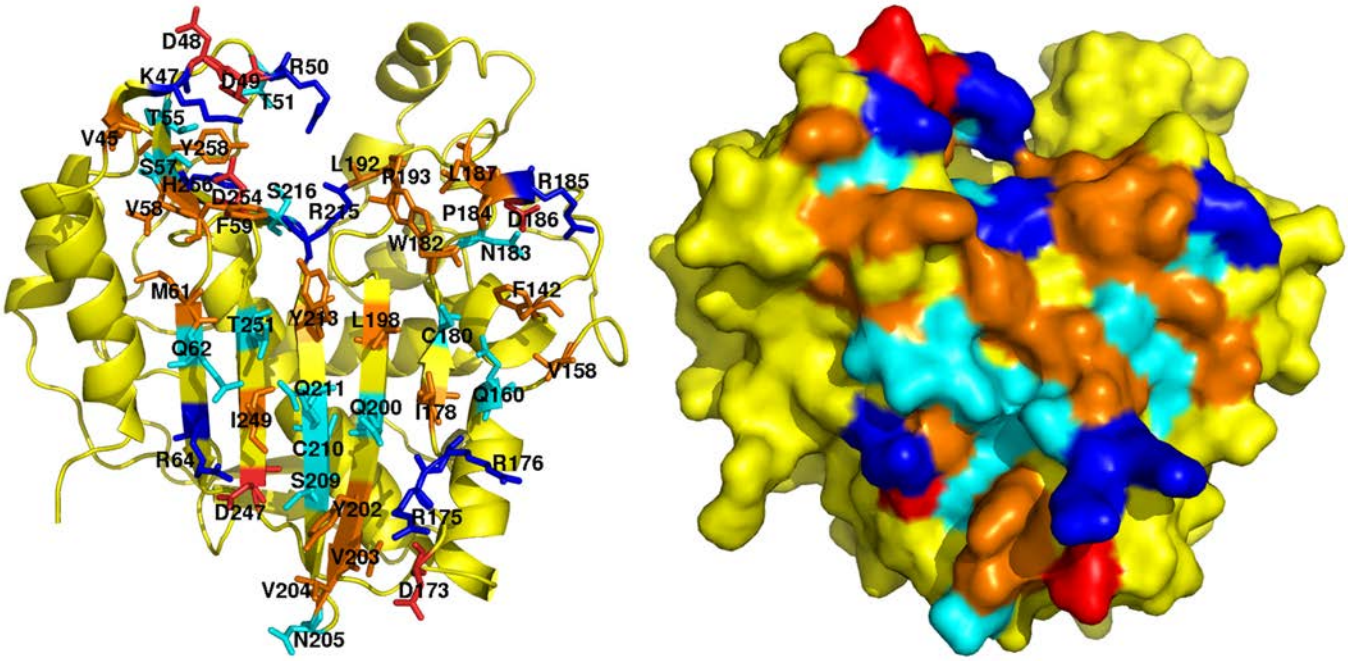

Figure S1. Residues at the monomer-monomer interface of hTS (PDB code 1HVY); left – backbone as cartoon and residues as sticks representation; right – molecular surface representation. One subunit is shown viewed from the direction of the second subunit. Color code: blue – positively charged (Arg, Lys, His); red – negatively charged (Asp); orange – hydrophobic/aromatic (Tyr, Trp, Leu, Ile, Met, Phe, Val, Pro); cyan – polar/neutral (Gln, Cys, Ser, Asn, Thr) residues. The presence of several arginines (R50, R64, R163, R175, R176, R185, R215) and aromatic residues (F59, F142, W182, Y202, Y213, Y258) can be observed. These types of residues are often enriched in hot spots. There is a high degree of conservation of the interface residues. Among the highly conserved residues are R50, R175, R176, I178, W182, L192, P194, R215, S216, H256, and Y258. On the other hand, the following interface residues are not conserved: V45, D48, M61, G143, R163, D173, D174, R185, D186, L189, V204, and N205.

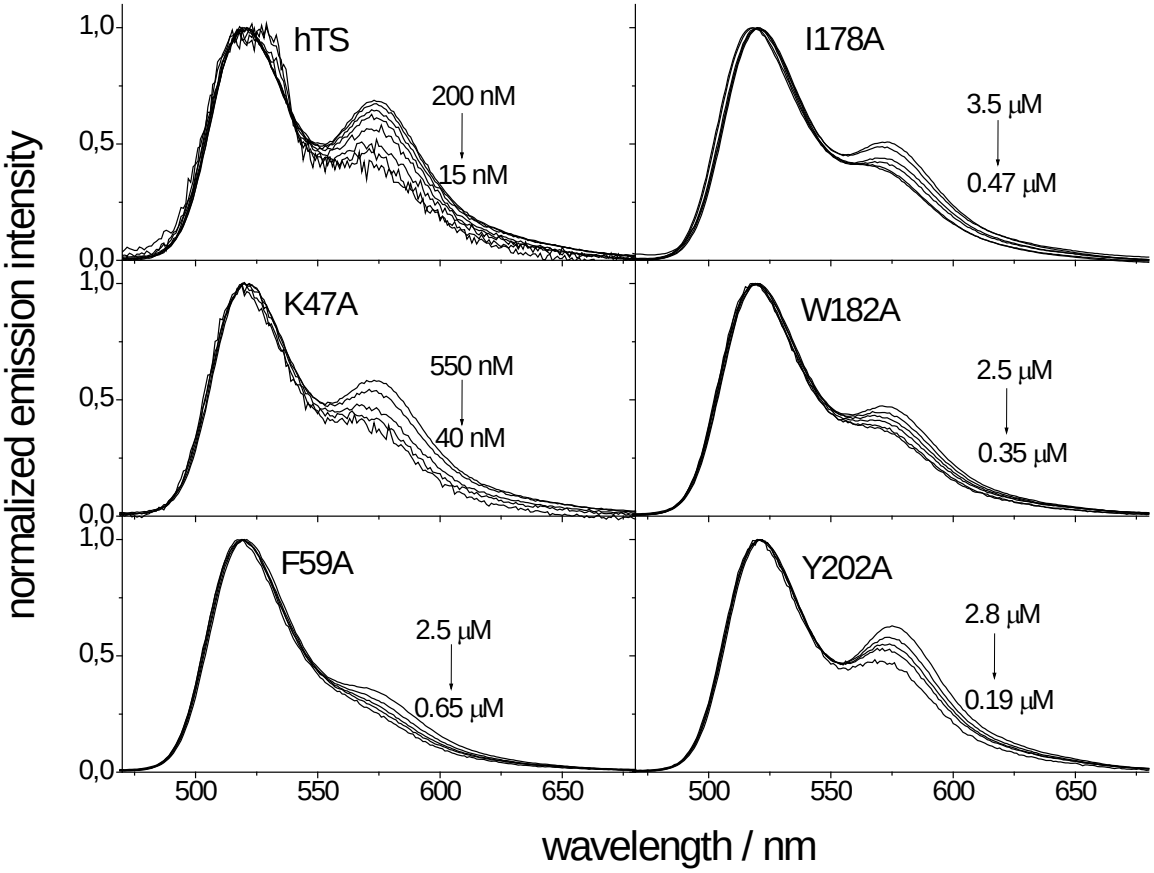

Figure S2. Emission spectra of hTS WT and five mutants at different total protein concentrations. λ_{exc} = 450 nm. The spectra are normalized at the maximum intensities for ease of comparison. Concentrations are given in M = moles of dimer per litre, and depended on the dimer stability of each protein.

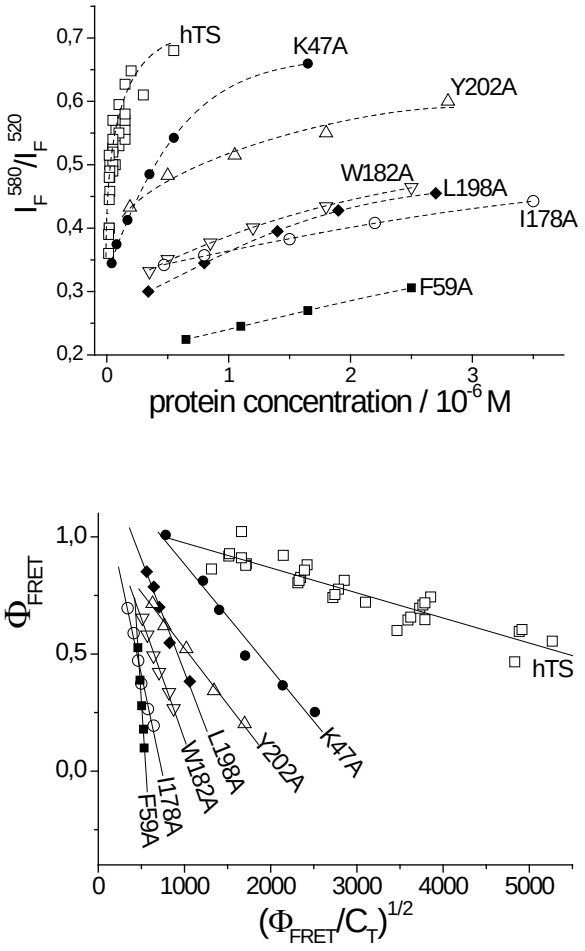

Figure S3. FRET analysis of the hTS WT and mutant proteins. (A) Ratios of fluorescence intensities at 580 nm (maximum of tetramethylrhodamine emission, I_F^{580}) and at 520 nm (maximum of fluorescein emission, I_F^{520}) as functions of total protein concentration (M, moles of dimer per litre). (B) Plots of equation 1 for hTS WT and six mutants. C_T is the total protein concentration in moles of dimers per litre. According to Eq.1, the slope gives the dimer dissociation constant, K_d.

A.

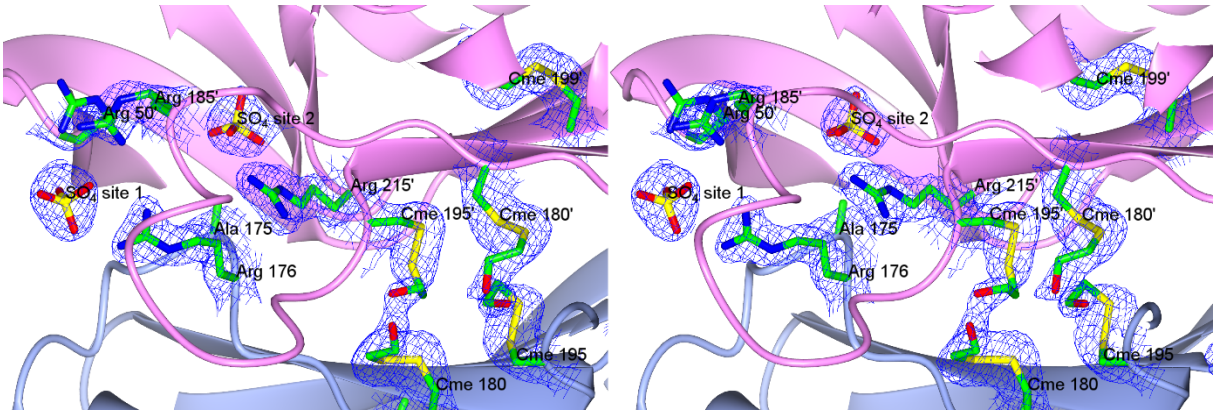

B.

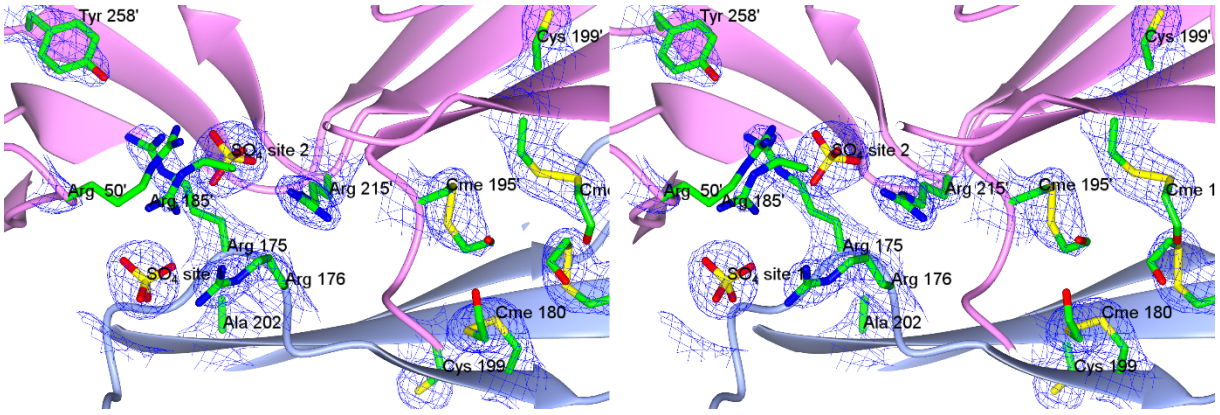

Figure S4. Stereo views of the interface between the two symmetry-related subunits in the crystal structures of the (**A**) R175A and (**B**) Y202A mutants of hTS. For details, see legend of Fig 5 (**a**,**c**).

Supporting Tables

Table S1. $\Delta\Delta G^0_s$ predictions for the change in stability of the hTS monomer fold upon mutation of the putative hotspot residues computed with the FoldX and Robetta web servers. Values in kJ/mol are given for both the A and B subunits of the 1HVY crystal structure of hTS in the active conformation and were computed for each protein subunit alone without bound ligands. Positive $\Delta\Delta G^0_s$ values indicate destabilization of the monomers.

Mutation	FoldX	Robetta	CUPSAT[a]
K47A	3.8/2.1	2.1/0.04	n.d.[b]
F59A	1.7/3.3	0.4/0.08	n.d.
R175A	1.7/0.8	-0.4/0.2	0.7/-2.5 (-2.1/-1.8)
I178A	7.5/9.2	7.1/7.5	n.d.
W182A	13.0/12.1	8.8/10.0	n.d.
L198A	5.9/7.1	4.2/6.3	n.d.
Y202A	2.9/5.0	1.3/2.5	n.d.
Y213A	8.0/8.0	5.9/6.3	n.d.

[a]Thermal method (corresponding values with the denaturant method in brackets); [b]not determined.

Table S2. Crystallographic data collection and refinement statistics for the R175A and Y202A variants of hTS. The data in parentheses refer to the highest resolution shell.

	hTS R175A PDB ID: 4KPW	**hTS Y202A PDB ID: 4JEF**
X-ray source	ID23-2 ESRF (Grenoble)	ALS 8.3.1 (Berkeley, US)
Wavelength (Å)	0.8726	1.1158
Data collection temperature (K)	100	100
Space group	$P3_121$	$P3_121$
Cell dimensions (Å)	96.32, 96.32, 82.69	95.95, 95.95, 82.65
Subunits/asu	1	1
Matthews coeff. ($Å^3Da^{-1}$)	3.03	3.14
Solvent Content (%)	59.41	60.86
Data reduction		
Resolution limits (Å)	37.24 – 2.03 (2.14 – 2.03)	50.00 - 2.31 (2.38 – 2.31)
Reflections measured	181366 (26523)	118604 (17352)
Unique reflections	29034 (4215)	19623 (1693)
Completeness (%)	99.9 (100.0)	99.5 (100.0)
R merge (%)	6.5 (39.6)	6.3 (67.0)
Multiplicity	6.2 (6.3)	6.0 (5.7)
$<I/\sigma(I>)$	16.1 (4.6)	25.1 (2.56)
Wilson B-factor ($Å^2$)	33.20	61.86
Refinement		
Resolution range (Å)	37.24-2.03 (2.10 - 2.03)	37.00-2.31 (2.43-2.31)
Reflections used	29020	19569
R cryst	16.10 (22.90)	18.50 (23.38)
R free; free R test set size	20.49 (29.74); 1475	22.20 (25.27); 1003
Total atoms (protein/ligand/water)	2330	2055
Protein atoms	2139	2028
Ethylene glycol molecules	3	0
Sulfate ions	3	3
Water molecules	164	24
Refinement type	Restrained refinement with TLS parameterization	Restrained refinement with TLS parameterization
Average B factor ($Å^2$)	46.56	76.86
r.m.s. deviation from ideal		
bond lengths (Å)	0.007	0.008
bond angles (°)	1.081	1.128
planar groups (Å)	0.005	0.005
chiral centres ($Å^3$)	0.078	0.070
e.s.d. (estimated standard deviation) in atomic positions (Å)	0.21	0.69
Ramachandran plot (%)		
Most favored	97.3	94.2
Allowed	2.7	5.0
Disallowed	0.0	0.8

Supporting Experimental Procedures

Materials

All chemical reagents were purchased from Sigma except for mTHF, which was generously provided by R. Moser (Merck Eprova AG).

Cloning and site-directed mutagenesis

Two separate 50 µL primer extension reaction mixtures (one each for forward and reverse primers, see list of primer couples for each mutant in the table below) were set up with 10 µL Phusion HF buffer, 1 µL 25 µM primer, 1 µL 10 nM dNTPs, 1 µL DNA template (the WT hTS), 36.5 µL ddH2O. Then 0.5 µL NEB Phusion polymerase was added. The initial denaturation step was set up for 30 s at 98 °C for PCR. The following cycles of the PCR reaction were repeated 4 times: denaturation (98 °C/10 s), annealing (55 °C/30 s) and extension (72 °C/15-30 s/kb bacterial DNA). After the final step, the samples were incubated at 72 °C for 5 min. Then 25 µL of the forward primer reaction and 25 µL of the reverse primer reaction were mixed, and 0.5 µL NEB Phusion polymerase was added. All the PCR cycles described above were repeated 25 times. Thereafter 25 µL of the reaction mixture was removed from the PCR instrument and incubated with 1 µL NEB DpnI at 37 °C for 3 hours. As a negative control, 0.5 µL DNA template in 25 µL H2O was digested with 1 µL NEB DpnI. Site-directed mutagenesis was confirmed by sequencing of the entire TS gene (ELIM Biopharmaceuticals Inc., Hayward, CA, US).

Primers for the hTS mutants

Mutation	Primer
K47A	CTGCGTTGTGGTGTTCGCGCGGATGATCGGACAGGTACC
F59A	ACCGGCACCTTAAGCGTCGCGGGCATGCAGGCGAGATAT
R175A	AAGACGAACCCGGATGATGCGAGAATCATAATGTGTGCT
I178A	CCGGATGATCGAAGAATCGCGATGTGTGCTTGGAACCCG
W182A	AGAATCATAATGTGTGCTGCGAACCCGCGCGATCTGCCG
L198A	CTTCCGCCATGCCATGCGGCGTGTCAATTTTACGTAGTC
Y202A	CATGCGCTGTGTCAATTTGCGGTAGTCAACAGTGAACTG
Y213A	GAACTGTCGTGCCAATTGGCGCAGCGTAGTGGCGACATG
C195S	CTCATGGCTCTTCCGCCAAGCCATGCGCTGTGTCAATTT
C195A	CTCATGGCTCTTCCGCCAGCGCATGCGCTGTGTCAATTT

Protein purification

WT hTS and all mutants were expressed in *E. coli* BL21(DE3) cells. Transformed bacteria were grown in standard Luria Broth culture medium at 37 °C and genetic selection was made by adding ampicillin (100 μg/mL). Protein expression was induced at OD_{595} nm = 0.4 – 0.8 with 0.4 mM IPTG (isopropyl-beta-D-thiogalactopyranoside). After 4 hours, cells were harvested by centrifugation at 5000 x g for 20 min at 4 °C, and the cell pellets were frozen at -20 °C. Cell lysis was done by repeated freezing and thawing, followed by sonication using Emulsiflex. The supernatant was separated from cell debris.

Proteins were purified using His-tag affinity purification (50 mM Tris pH 6.9 (RT), 300 mM KCl, eluted with 500 mM imidazole) and subsequently by size-exclusion chromatography (50 mM Tris pH 6.9 (RT), 300 mM KCl). Purification was confirmed by SDS-PAGE gel. The purified protein was stored at –80 °C.

All mutants were analyzed by mass spectrometry. For accurate mass measurement, ESI-Q-Tof analysis was performed (6520 Accurate-Mass Q-Tof – Agilent Technologies). The MassHunter program (B.02.00, Agilent Technologies) was used for deconvolution (Maximum Entropy method). All mutant proteins were digested with trypsin and the spectra were acquired using both MALDI (4800 Plus MALDI TOF/TOF, Applied Biosystems) and nanoLC- ESI-Q-Tof (Agilent Technologies) mass spectrometers. MS and MS/MS spectra were analyzed by using the free Mascot software (www.matrixscience.com). Peptides containing the mutation were observed by MALDI and/or ESI-MS. The gel electrophoresis and mass spectrometry showed that the proteins were purified to more than 90% purity.

FRET assays and analysis of mutant data

Each mutant was labelled with an excitation-energy donor-acceptor pair, fluorescein (F) and tetramethylrhodamine (T). The FRET signal, consisting of acceptor emission upon donor excitation, occurs only from the dimeric protein and was used to monitor the dimer/monomer equilibrium. Quantitative analysis of FRET efficiency as a function of total protein concentration yielded the K_d values and the corresponding ΔG_d^0 values.

Conjugation of the mutants to the fluorescent probes, F and T, was carried out as described in (Genovese et al., 2010) at room temperature, 24-26 °C. UV-visible absorption spectra were measured with a Varian Cary 100 spectrophotometer. The concentrations of the two probes and of the protein were determined by separating their absorbance contributions at the maxima: 500 nm (ε_F = 79000 M^{-1} cm^{-1}), 557 nm (ε_T = 103000 M^{-1} cm^{-1}), 280 nm (ε_{hTS} = 89000 M^{-1} cm^{-1}). Fluorescence spectra were measured on a Spex-Jobin Yvon Fluoromax2 spectrofluorometer with 0.4 (emission direction) x 1 (excitation direction) cm^2 cuvettes. F and T maximum absorbencies were kept below 0.1 (with an optical path of 1 cm) to make deformations of emission spectra due to inner filter effects negligible.

The anomalous emission behaviour of the R175A mutant can be accounted for on the basis of simple statistics applied to a fully dissociated protein dimer with three conjugatable cysteine residues per monomer. The observed ratio of the T probe contribution at 580 nm to the F probe contribution at 520 nm is 0.35-0.4 for a fully associated hTS dimer; it is 1.1-1.2 for the R175A mutant. Thus it increases by a factor of 3. For a fully dimeric hTS, the probe-conjugated dimers are present in the ratios FF:FT:TT = 1:2:1. Under the reasonable assumption of complete FRET within a dimer and neglecting the directly excited T emission (TT) (see (Genovese et al., 2010)), the F emission will derive from FF (2, the number of fluorophores, x 1, the abundance of the species) and T emission from FT (1 x 2), yielding a T-to-F ratio of 1 (here it is not necessary to take into account the different quantum yields of the two probes). Based on the spectrophotometric finding of three probes per protein monomer, if we assume R175A to be fully dissociated into monomers, FRET to be complete within a monomer and the two probes to have equal affinities for the accessible cysteine residues (as indicated by the UV-visible absorption spectral evidence, F:T=1:1), then we will have FFF:FFT:FTT:TTT = 1:3:3:1. Thus F will emit 3 (3 x 1, the abundance of FFF) and T will emit 9 (2 x 3 from FFT + 1 x 3 from FTT); the T-to-F emission ratio will therefore rise by a factor 3, as experimentally observed.

Circular Dichroism (CD)

The CD spectra of WT and mutant hTS were measured at room temperature (ca. 25 °C) on a Jasco J-810 spectropolarimeter. Samples were in 0.1 cm cuvettes and had maximum absorbances around 1 at ca. 195 nm. Phosphate buffer (pH 7.5) signals were subtracted but no other correction was introduced. Protein concentrations determined spectrophotometrically and the number of residues per protein dimer (650) was used to derive the $\Delta\varepsilon$ spectra in the peptide absorption region. These were analyzed using the CDSSTR program (Sreerama and Woody, 2000) on the Dichroweb site (http://dichroweb.cryst.bbk.ac.uk) (Whitmore and Wallace, 2004, 2008) in combination with the SP175 reference data sets.

Crystallization

1) R175A mutant:

The histidine tagged construct of the hTS R175A mutant used consisted of the whole human sequence (UniProt entry: P04818) with the MRGSHHHHHHGS sequence added at the N-terminus making a total of 325 residues (MW=37114.45 kDa: the residue numbering refers to the WT hTS sequence, excluding the N-terminal tag) (Cardinale et al., 2011). Crystals were grown using the hanging drop vapor diffusion technique at room temperature (Benvenuti and Mangani, 2007). Drops were prepared by mixing 3 μL of R175A mutant solution (130 μM in 100 mM HEPES, pH 7.5) with 1.5 μL of a precipitant solution (30-40 % saturated ammonium sulfate, 20 mM β-ME and 0.1 M Tris-HCl at pH 8.8) and inverted over a 600 μL reservoir. Crystals isomorphous to the native enzyme grew in 10-14 days. Before data collection, the crystals were transferred to a cryoprotectant solution constituted by 20% ethylene glycol added to the precipitant solution and then flash frozen in liquid nitrogen.

2) Y202A mutant:

The Y202A mutant was co-crystallized with a weak inhibitory compound with a mixed-type mechanism similar to a previously characterized thiazole derivative (Carosati et al., 2012). The protein (in 100 mM HEPES pH 7.5 at 4 °C) was concentrated at 1.5 mg/mL, mixed with the inhibitor at a ratio of 1:15 and then incubated for about 1h on ice. Hexagonally shaped crystals in the $P3_121$ space group grew in 2.0 M ammonium sulfate, 20 μM β-ME and 0.1 M Mes, pH 6.5, 5% (w/v) Peg400 at room temperature. They were grown in hanging drops by the vapor diffusion method using a Mosquito workstation (TTP Labtech). Hexagonal crystals in the $P3_121$ space group grew in 2-14 days at room temperature. Before data collection, the crystals were transferred to a cryoprotectant solution constituted by 20% ethylene glycol added to the precipitant solution and then flash frozen in liquid nitrogen.

Crystal structure determination

1) R175A mutant:

Crystallographic diffraction experiments were carried out at the ESRF (European Synchrotron Radiation Facility, Grenoble, France) beamline ID23-2 on cryocooled crystals (100 K). A complete data set was recorded from a single crystal using the rotation technique ($\Delta\varphi = 1°$) at a fixed wavelength (0.8736 Å) on a MAR mosaic 225 CCD detector. Data were indexed and

processed using MOSFLM 7.0.6 (Leslie, 2006) and scaled with SCALA (Evans, 2006) from the CCP4 (Winn et al., 2011). Crystals of the R175A variant belong to the trigonal space group $P3_121$, as previously observed for the native enzyme crystallized in similar conditions, with one enzyme subunit in the asymmetric unit. The structure of the native enzyme in the inactive conformation (PDB ID: 3N5G), was used as a search model for the molecular replacement carried out using the software MOLREP (Vagin and Teplyakov, 2000). Crystallographic refinement was performed with the program PHENIX (Adams et al., 2002; Afonine et al., 2012). The graphics software Coot (Emsley and Cowtan, 2004; Emsley et al., 2010) was used to visualize the structure and for manual rebuilding and modeling of missing atoms into the electron density maps. Water molecules were added using the program ARP/wARP (Langer et al., 2008) and checked both manually and by the automatic procedures within Coot. The Translation/Libration/Screw (TLS) refinement (Painter and Merritt, 2006a) was introduced in the final maximum-likelihood refinement cycles. The optimal partitioning of the refined R175A structure was determined through the TLS Motion Determination web server (Painter and Merritt, 2006a; Painter and Merritt, 2006b) and the partitioning scheme consisted of eight continuous segments.

2) Y202A mutant:

X-ray diffraction data were collected from cryo-protected crystals (in 20% ethylene glycol) at the Beamline 8.3.1 of the Advanced Light Source (Lawrence Berkeley National Laboratories) on a 315r CCD detector. The hexagonal crystals diffracted to 2.3 Å resolution. Reflections were indexed, reduced, and scaled with *HKL2000* (Otwinowski and Minor, 1997). The structure was determined by molecular replacement in Phaser (Storoni et al., 2004) using human TS (1HVY) as a search model. Model building was done using Coot. Restrained positional refinement and refinement of isotropic B-factors and TLS parameters were done using REFMAC5 (Murshudov et al., 1997) from the CCP4 suite (CCP4, 1994) and PHENIX.

Four of the five cysteine residues in the mutants reacted with β-ME to give covalent adducts, In the R175A mutant, three cysteines (C180, C195 and C199) were modeled as S,S-(2-hydroxyethyl)thiocysteine, whereas, for C43, only a S-C fragment was visible in the electron density maps and modeled. The only cysteine residue that remained unreacted was C210 which is buried. In the Y202A mutant, only two cysteines (C180 and C195) were oxidized. The reactivity

of hTS cysteines with β-mercaptoethanol (β-ME) molecules has been previously observed and described (Cardinale et al., 2011; Phan et al., 2001).

Like all hTS crystal structures found in the inactive conformation, there were disordered regions not visible in the electron density maps. In the R175A structure, loop 107-128 and the N- and C-termini (the N-terminus tag, residues 1-25 and residues 311-313) were not visible. The Y202A mutant was co-crystallized with a small molecule with a partially disordered binding mode, similar to that observed by Carosati et al. (2012) for a mixed-type inhibitor molecule with WT hTS, close to the active site and overlapping with the binding site for the PABA-Glu moiety of mTHF. However, the electron density for this inhibitor was not sufficiently well defined to build it into the structure. The eukaryotic insert (residues 102-132) was not visible in the electron density map and the density for the insert corresponding to residues 142-153 was weak and broken. The residues connecting these two inserts were in a conformation that contacted the cofactor binding site as observed by Carosati et al. (2012).

The stereochemical quality of the final models was checked using the PROCHECK software (Laskowski et al., 1993). Figures were generated using the molecular graphics program CCP4mg (McNicholas et al., 2011). Data collection, processing statistics, *R*-factors and final models are listed in **Table S2.**

References

Adams, P.D., Grosse-Kunstleve, R.W., Hung, L.W., Ioerger, T.R., McCoy, A.J., Moriarty, N.W., Read, R.J., Sacchettini, J.C., Sauter, N.K., and Terwilliger, T.C. (2002). PHENIX: building new software for automated crystallographic structure determination. Acta Crystallogr. D Biol. Crystallogr. *58*, 1948-1954.

Afonine, P.V., Grosse-Kunstleve, R.W., Echols, N., Headd, J.J., Moriarty, N.W., Mustyakimov, M., Terwilliger, T.C., Urzhumtsev, A., Zwart, P.H., and Adams, P.D. (2012). Towards automated crystallographic structure refinement with phenix.refine. Acta Crystallogr. D Biol. Crystallogr. *68*, 352-367.

Benvenuti, M., and Mangani, S. (2007). Crystallization of soluble proteins in vapor diffusion for x-ray crystallography. Nat. Protoc. *2*, 1633-1651.

Cardinale, D., Guaitoli, G., Tondi, D., Luciani, R., Henrich, S., Salo-Ahen, O.M., Ferrari, S., Marverti, G., Guerrieri, D., Ligabue, A., Frassineti, C., Pozzi, C., Mangani, S., Fessas, D., Guerrini, R., Ponterini, G., Wade, R.C., and Costi, M.P. (2011). Protein-protein interface-binding peptides inhibit the cancer therapy target human thymidylate synthase. Proc. Natl. Acad. Sci. USA *108*, E542-549.

Carosati, E., Tochowicz, A., Marverti, G., Guaitoli, G., Benedetti, P., Ferrari, S., Stroud, R.M., Finer-Moore, J., Luciani, R., Farina, D., Cruciani, G., and Costi, M.P. (2012). Inhibitor of ovarian cancer cells growth by virtual screening: a new thiazole derivative targeting human thymidylate synthase. J. Med. Chem. *55*, 10272-10276.

CCP4. (1994). The CCP4 suite: programs for protein crystallography. Acta Crystallogr. D Biol. Crystallogr. *50*, 760-763.

Emsley, P., and Cowtan, K. (2004). Coot: model-building tools for molecular graphics. Acta Crystallogr. D Biol. Crystallogr. *60*, 2126-2132.

Emsley, P., Lohkamp, B., Scott, W.G., and Cowtan, K. (2010). Features and development of Coot. Acta Crystallogr. D Biol. Crystallogr. *66*, 486-501.

Evans, P. (2006). Scaling and assessment of data quality. Acta Crystallogr. D Biol. Crystallogr. *62*, 72-82.

Genovese, F., Ferrari, S., Guaitoli, G., Caselli, M., Costi, M.P., and Ponterini, G. (2010). Dimer-monomer equilibrium of human thymidylate synthase monitored by fluorescence resonance energy transfer. Protein Sci. *19*, 1023-1030.

Langer, G., Cohen, S.X., Lamzin, V.S., and Perrakis, A. (2008). Automated macromolecular model building for X-ray crystallography using ARP/wARP version 7. Nat. Protoc. *3*, 1171-1179.

Laskowski, R.A., Moss, D.S., and Thornton, J.M. (1993). Main-chain bond lengths and bond angles in protein structures. J. Mol. Biol. *231*, 1049-1067.

Laue, T.M. (1995). Sedimentation equilibrium as thermodynamic tool. Methods Enzymol. *259*, 427-452.

Leslie, A.G. (2006). The integration of macromolecular diffraction data. Acta Crystallogr. D Biol. Crystallogr. *62*, 48-57.

McNicholas, S., Potterton, E., Wilson, K.S., and Noble, M.E. (2011). Presenting your structures: the CCP4mg molecular-graphics software. Acta Crystallogr. D Biol. Crystallogr. *67*, 386-394.

Murshudov, G.N., Vagin, A.A., and Dodson, E.J. (1997). Refinement of macromolecular structures by the maximum-likelihood method. Acta Crystallogr. D Biol. Crystallogr. *53*, 240-255.

Otwinowski, Z., and Minor, W. (1997) Processing of X-ray diffraction data collected in oscillation mode. In Methods Enzymol., C.W. Carter, Jr., ed. (Academic Press), pp. 307-326.

Painter, J., and Merritt, E.A. (2006a). Optimal description of a protein structure in terms of multiple groups undergoing TLS motion. Acta Crystallogr. D Biol. Crystallogr. *62*, 439-450.

Painter, J., and Merritt, E.A. (2006b). TLSMD web server for the generation of multi-group TLS models. J. Appl. Cryst. *39*, 109-111.

Phan, J., Steadman, D.J., Koli, S., Ding, W.C., Minor, W., Dunlap, R.B., Berger, S.H., and Lebioda, L. (2001). Structure of human thymidylate synthase suggests advantages of chemotherapy with noncompetitive inhibitors. J. Biol. Chem. *276*, 14170-14177.

Storoni, L.C., McCoy, A.J., and Read, R.J. (2004). Likelihood-enhanced fast rotation functions. Acta Crystallogr. D Biol. Crystallogr. *60*, 432-438.

Vagin, A., and Teplyakov, A. (2000). An approach to multi-copy search in molecular replacement. Acta Crystallogr. D Biol. Crystallogr. *56*, 1622-1624.

Winn, M.D., Ballard, C.C., Cowtan, K.D., Dodson, E.J., Emsley, P., Evans, P.R., Keegan, R.M., Krissinel, E.B., Leslie, A.G., McCoy, A., McNicholas, S.J., Murshudov, G.N., Pannu, N.S., Potterton, E.A., Powell, H.R., Read, R.J., Vagin, A., and Wilson, K.S. (2011). Overview of the CCP4 suite and current developments. Acta Crystallogr. D Biol. Crystallogr. *67*, 235-242.